Enantioselective Decarboxylative C(sp^3)-C(sp^3) Cross-Coupling of Aliphatic Acids with *gem*-Borazirconocene Alkanes

Authors: Jing Wang[1,2,3], Songlin Bai[1,2,3], Chao Yang[4], Xiangbing Qi[2,3]*

Affiliations:

[1]School of Life Sciences, Tsinghua University, Beijing 100084, China.

[2]National Institute of Biological Sciences, 7 Science Park Road, Zhongguancun Life Science Park, Beijing 102206, China.

[3]Tsinghua Institute of Multidisciplinary Biomedical Research, Tsinghua University, Beijing 100084, China.

[4]Celluranics New Materials Co., No. 18-28, Tongjiang Road, Taixing Economic and Technological Development Zone, Taizhou City, Jiangsu Province, China.

* Corresponding author. Email: qixiangbing@nibs.ac.cn (X. Q.)

Abstract:

Asymmetric decarboxylative cross-couplings of carboxylic acids represent a powerful tool for synthesizing chiral building blocks for medicinal chemistry and material science. However, the synthesis of versatile chiral alkylboron derivatives via asymmetric decarboxylative C(sp^3)-C(sp^3) cross-coupling from readily available primary aliphatic acids and mild organometallic reagents is still challenging. In this study, we report a visible-light-induced, Ni-catalyzed enantioconvergent C(sp^3)-C(sp^3) cross-coupling of unactivated primary aliphatic acids with *gem*-borazirconocene alkanes, furnishing a diverse array of valuable chiral alkylboron building blocks. The broad substrate scope, high functional group tolerance, and the late-stage modification of complex drug molecules and natural products with high enantioselectivity demonstrate the synthetic potential of the method. Mechanistic investigations suggest an enantioconvergent radical-radical cross-coupling pathway, wherein the primary radical from carboxylic acids is generated through single-electron reduction with Zr^{III} species, representing an unprecedented example of enantioselective radical C(sp^3)-C(sp^3) cross coupling in the absence of photocatalysts.

Introduction

Benefiting from the widespread commercial availability, lower toxicity, and stability of aliphatic acids, the past decades have witnessed a wealth of transition-metal-catalyzed decarboxylative cross-coupling to forge new C-C and C-X bonds. The high levels of chemoselectivity and functional group tolerance exhibited by these reactions have enabled the late-stage C(sp^3)-enriched functional group modification and spatial diversification of bioactive molecules and natural products[1–11]. A great progress has been made in efficiently constructing racemic C(sp^3)-C(sp^3) bonds via transition metal catalyzed decarboxylative cross-coupling of aliphatic acids. Various strategies have been developed by groups led by MacMillan[12–15], Baran [11,16–19], Fu [20], Weix [21], and Cernak [22] etc., encompassing diverse cross-coupling partners such as alkyl halides, alkenes, alcohols, amines, and even carboxylic acids. Despite these advancements, achieving asymmetric decarboxylative couplings with C(sp^3) partners remains a formidable challenge[1,5–7,23].

In 2023, the Baran's group developed a Ni-electrocatalytic enantioselective doubly decarboxylative cross coupling (dDCC), radicals that are derived from malonate half amide and aliphatic acid were generated via single electron-transfer (SET) from Ni(I) to redox-active aliphatic acid NHPI (N-hydroxyphthalimide) esters (**Figure 1A, 1**)[24]. Recently, the Yang's group disclosed a cooperative photoredox/Fe/chiral primary amine triple catalysis protocol to construct quaternary stereocenters by decarboxylative cross-coupling of 1,3-dicarbonyl compounds with primary alkyl radical, which was generated from the reduction of aliphatic acid NHPI esters (**Figure 1A, 2**) by an iridium photocatalyst [25].

Both cases demonstrate the feasibility of enantioconvergent decarboxylative C(sp^3)-C(sp^3) cross-coupling using reactive primary radical species. The Fu's group realized the asymmetric decarboxylative Negishi cross-coupling reaction of *α*-amino acid-derived NHPI esters[26] (**Figure 1A, 3**). Subsequently, the Baran's group further demonstrated asymmetric decarboxylative Negishi-type alkylation of *α*-oxy carboxylic acids[27] (**Figure 1A, 4)**. These two methodologies showcase the potent combination of decarboxylation of *α*-heteroatom-substituted carboxylic acids with organometallic reagents in an enantioselective pathway.

Compared to *α*-heteroatom and *α*-carbonyl stabilized radicals, the enantioconvergent C(sp^3)-C(sp^3) cross-coupling of primary radicals via decarboxylation of unactivated primary aliphatic acids remains underexploited[7,25]. Additionally, the selection of organometallic partners in asymmetric decarboxylative cross-coupling is largely confined to alkylzinc reagents, which typically involve tedious synthesis procedures such as oxidative insertion into alkyl halides by zinc or transmetalation using zinc salts. These methods suffer from harsh conditions, and a limited substrate scope, restricting their practical utility[28,29]. Hence, the application of easily prepared and mild organometallic reagents in asymmetric decarboxylative C(sp^3)-C(sp^3) cross-coupling is highly desirable.

We inquire whether the asymmetric decarboxylative C(sp^3)-C(sp^3) cross-coupling reactions could employ moderate organometallic reagents to install versatile chiral alkylboron derivatives，which possess a diverse reactivity profile crucial for drug discovery and material sciences[30–33]. Considerable effort has been devoted to exploring synthetic methodologies for the preparation of these scaffolds[34–38]. Among them, asymmetric transformations of abundant and easily accessible feedstock chemicals offer an appealing synthetic platform toward chiral alkylboron derivatives but remain elusive. Pioneering works by Li[39], Baran[40], Aggarwal[41] and substantial progress[42–52] on decarboxylative borylation of aliphatic acids underscore the reliability of decarboxylative reactions in synthesizing alkylboron derivatives. Nevertheless, methods for constructing chiral alkylboron derivatives via asymmetric decarboxylative cross-coupling reactions[53] of unactivated primary aliphatic acids have yet to be reported.

The deployment of alkylzirconocenes has emerged as a powerful platform for the construction of valuable C(sp^3)-C(sp^3) bonds[54–59]. This versatile organometallic specie demonstrates exceptional functional group tolerance, unique photochemical reactivity, and the capacity to facilitate remote C-H functionalization through their intriguing "chain-walking" ability. Notably, alkylzirconocenes can be readily prepared from abundant and readily available feedstock chemicals, such as alkenes[60–62]. The confluence of these desirable reactivity features and their synthetic accessibility renders alkylzirconocenes highly attractive synthetic intermediates for the efficient assembly of complex molecular architectures. The ongoing exploration of the photoreactivity exhibited by alkylzirconocenes has opened up new avenues for the development of asymmetric photoredox methodologies[63–67]. Recognizing the advantages of both aliphatic acids and alkylzirconocenes, we have developed a visible-light-induced, Ni-catalyzed enantioconvergent C(sp^3)-C(sp^3) cross-coupling of unactivated primary aliphatic acid NHPI esters with *gem*-borazirconocene alkanes, yielding a diverse range of chiral alkylboron derivatives (**Figure 1B**). Mechanistic investigations point to an enantioconvergent radical-radical cross-coupling mechanism, wherein the primary radical from carboxylic acid is generated through single-electron reduction by Zr^{III} species.

Results

We initiated our investigation into asymmetric C(sp^3)-C(sp^3) cross-coupling using ethyl *gem*-borazirconocene with NHPI ester **1a** under blue light-emitting diodes (LEDs) irradiation. After extensive screening of Ni catalysts, chiral ligands, additives, and solvents (for detailed optimization studies, see **Supplementary Table 2-6**), the best result was obtained affording **3a** in 76.0% isolated yield and 91.0%

enantiomeric excess (ee). However, the use of long-chained *gem*-borazirconocene alkanes led to diminished enantioselectivity. Recognizing the critical role of ancillary ligand in modulating reaction cross-selectivity, and enantioselectivity, we focused on ligand optimization for octyl *gem*-borazirconocene with NHPI ester **1a**. A series of diamine ligands were examined, and the desired C(sp^3)-C(sp^3) cross-coupling was successfully achieved in the presence of $Ni(BF_4)\cdot 6H_2O$ (10 mol%), chiral ligand **L6** (12 mol%), tetrahydrofuran (THF, 0.1 M) under 0.5 W blue LEDs irradiation at 4ºC, yielding chiral alkylboron product **4b** in 82.0% isolated yield and 91.6% ee (**Table 1**, entry 1 and **Supplementary Table 7**). Control experiments confirmed the necessity of the Ni catalyst, visible light, and *gem*-borazirconocene alkanes for optimal reaction performance (**Table 1**, entries 2-4 and **Supplementary Figure 1**). Ligands with different substitutions at nitrogen atoms (**L1**, **L2**, **L3**) or different aryl groups (**L4**, **L5**, **L7**) were found to be less effective than **L6** (**Table 1**, entries 4-10).

With the optimal conditions established, we explored the generality of this transformation by investigating a wide range of aliphatic acids (**Figure 2**). The NHPI esters containing a variety of aryl halides (**3b**, **3g**, **3i**, **3l**) were well tolerated and a trifluoromethyl group (**3c**) was also proved suitable for the reaction. Electron-rich methyl substitutions at the para- (**3d**), meta- (**3k**) and ortho- position (**3h**) of the aryl ring, as well as di-substituted methoxyl substrates (**3j**), yielded products with excellent enantiomeric excess and yield. Ester (**3e**), sulfonamide (**3f**), and imide (**3q**) were also compatible with the reaction conditions. Notably, a bulky naphthalene-substituted NHPI ester exhibited slightly reduced reactivity and enantioselectivity (**3m**). Besides aryl groups, biologically relevant heterocycles such as thiophene (**3n**), furan (**3o**), and indole (**3p**) were amenable. Long-chained alkyl sulfonamide (**3r**) substrate was accommodated with good yield and enantioselectivity. It was noteworthy that unprotected indole substrate afforded modest yield and good enantiomeric excess (**3p**) under this condition. The remarkable functional group tolerance of the method suggests its potential to modify complex bioactive molecules. A range of pharmaceutical agents were successfully functionalized, including the direct modification of immunosuppressant agent mycophenolic acid (**3s**), chemotherapy drug chlorambucil (**3t**), and bile acids such as chenodeoxycholic acid (**3u**) and dehydrocholic acid (**3v**), highlighting the potential utility of this protocol for late-stage functionalization of complex molecules.

Next, the scope of *gem*-borazirconocene alkanes was evaluated (**Figure 2**). The asymmetric catalysis exhibited insensitivity to the chain length of *gem*-borazirconocene alkanes (**3a**, **4b-c**). A wide range of functional groups such as alkyl chloro (**4d**), silane (**4g**), ether (**4k**), sulfonamide (**4i**), and indole (**4j**) were well-tolerated. The reactivity and enantioselectivity of the reaction were influenced by the steric hindrance of *gem*-borazirconocene alkanes. The bulky substrates (**4e**, **4f**, **4g**, **4l**) gave lower yields and enantioselectivity, as evidenced by the comparison between **4h** and **4l**. The protocol could also be applied to several bioactive molecules including glucose (**4m**), cholesterol (**4o**), and DL-alpha-Tocopherol (**4n**), highlighting the high functional-group tolerance of the method. By harnessing the Bpin directed "chain-walking" effect, the general terminal or internal alkenes can be converted into *gem*-borazirconocene alkanes to realize remote C-H functionalization[67]. The terminal alkene substrates (**4p**, **4q**) were successfully transformed into *gem*-borazirconocene alkanes and performed excellently in the decarboxylative cross-coupling with high enantioselectivity, further demonstrating the broad substrate scope of this method.

Chiral alkylboron derivatives are versatile building blocks for asymmetric synthesis, they can be stereospecifically transformed into a range of functional groups, providing access to diverse molecules with high enantioselectivity[68]. To further show the synthetic potential of this asymmetric decarboxylative reaction, a 1.5 mmol scale experiment was conducted, yielding **3a** in comparable yield although using a

lower equivalent ethyl *gem*-borazirconocene (2.5 equiv. versus 3.7 equiv.) (**Figure 3A**). The C(sp^3)-B bond of the resulting chiral product was subsequently transformed to a new C(sp^2)-C(sp^3) bond through stereospecific 1,2-boryl migration[69] (**Figure 3B**, **5a**). Additionally, it can be converted into a series of carbon-heteroatom bonds. The oxidation of **3a** afforded secondary alcohol **5b**. Amination with the H_2N-DABCO reagent forged a new C-N[70] bond (**5c**). The stereospecific bromination of **3a** produced alkyl bromide product **5d**, which could readily undergo further functional group interconversions[71].

Discussion

A series of experiments were conducted to gain insight into the mechanism. Radical clock probes **6** and **7** were subjected to the standard conditions, yielding the cyclopropane ring-opening/coupling product **4k-2** and hept-6-enoic acid decarboxylative cyclization/coupling product **4k-3** (**Figure 4A**). These outcomes suggested the involvement of an open-shell alkyl radical generated from NHPI esters. Previous research demonstrated that racemic *gem*-borazirconecene alkane reagents generated the alkyl radicals under blue LEDs irradiation in a stereoconvergent manner[64]. The combined results strongly support the hypothesis that the decarboxylative cross-coupling occurs through a radical-radical cross-coupling mechanism. Control experiments revealed that the decarboxylation could not be triggered without visible light and *gem*-borazirconecene alkane (**Figure 4B** and **Supplementary Figure 1**). The decarboxylative byproduct **3ab** was detected without Ni-ligand complex. Light on/off experiment showed that the reactions were shut down when the blue LEDs was turn off (**Supplementary Figure 10** and **11**), ruling out the radical chain mechanism.

As $Cp_2Zr^{III}Cl$ species was proven to be a strong single-electron reductant[63,64,66], it has the potential to reduce the NHPI esters instead of low-valent Ni[72]. To determine the actual reductant, the initial-rate method was employed to determine the kinetics of **1a**, ethyl *gem*-borazirconecene and Ni catalyst under standard conditions. Zero-order rate dependences on NHPI ester **1a** and the Ni catalyst (**Supplementary Figure 13**, **17**), and a first order dependence on *gem*-borazirconocene (**Supplementary Figure 15**) were observed. To further elucidate the mechanistic details of the radical decarboxylative process, the conversion rate of NHPI ester **1a** was monitored under varying loading of the Ni catalyst and the ethyl *gem*-borazirconocene reagent[73]. The results showed that the conversion of **1a** was independent of Ni catalyst loading (**Supplementary Figure 3**). A positive correlation between the consuming rate of **1a** and borazirconocene alkanes concentration was observed (**Supplementary Figure 5**). According to the kinetics results, we proposed that the reduction of NHPI esters was independent of the Ni catalyst, suggesting the $Cp_2Zr^{III}Cl$ mediated reduction might be a major pathway.

The study of the effect of ligand enantiopurity on the product enantioselectivity revealed a linear relationship (**Figure 4C**), suggesting the involvement of a single chelating ligand **L6** in the enantiodetermining step. The absolute configuration of product **3a** generated under the Ni/((*R,R*)-**L6**) reaction conditions was determined to be the *R* configuration, as confirmed by the X-ray crystallographic analysis of derivative **5b-1** (CCDC number: 2347391). Based on the accumulated experimental evidence, two possible mechanistic pathways can be proposed for this asymmetric decarboxylative C(sp^3)-C(sp^3) cross-coupling reaction: “Transmetallation (TM) First” pathway or the “Single-electron oxidative addition (SOA) First” pathway. In the SOA first pathway (**Figure 4D**), a chiral Ni^{II} species (**I**) was first reduced to the reactive Ni^{I} intermediate (**II**) by the Zr^{III} species, which was generated from the homolysis of *gem*-borzirconocene alkane (**d**) under blue LEDs irradiation. The primary radical (**b**) derived from NHPI esters was captured by the Ni^{I} (**II**) intermediate to furnish complex **III**, which can intercept with the resulting alkylboron radical (**c**) to give complex **IV**. This Ni^{III} species underwent reductive elimination to deliver the enantioenriched alkylboron product (**e**).

To elucidate the proposed mechanism and gain a deeper understanding of the enantioselectivity-determining step, density functional theory (DFT) calculations were performed. The radical-type organozirconocene-based C(sp^3)-C(sp^3) cross-coupling mechanism has been previously elucidated in our previous studies[63,64]. In the present decarboxylative cross-coupling system, $Ni(BF_4)_2 \cdot 6H_2O$ was identified as the optimal nickel source. Compared to previous reaction conditions, this system did not involve any halide anion. We compared three possible Ni^I complexes with different counter ions and found that the phthalimide anion (**1-3**, 0.0 kcal/mol) was thermodynamically more stable compared to THF (**1-2**, 25.0 kcal/mol) or BF_4 (**1-1**, 25.9 kcal/mol) (**Supplementary Figure 63**).

Based on the Phthalimide-Nickel model, we conducted DFT computations on the two proposed pathways: the “TM First” pathway and the “SOA First” pathway. In the "TM First" pathway (**Figure 5A**), the alkylboron radical was initially added to the Ni^I species, resulting in the formation of two diastereomeric intermediates, **2-1** and **2-2**, via two closely related transition states (**2-1_TS** 2.4 kcal/mol and **2-2_TS** 2.4 kcal/mol). The subsequent alkyl radical addition to the Ni^{II} intermediates exhibited low energy barriers (**3-1_TS2** 3.0 kcal/mol, **3-2_TS2** 5.0 kcal/mol). Finally, intermediate **3-1** and **3-2** underwent reductive elimination to generate products through irreversible exothermic processes. In this pathway, the alkylboron radical addition step dominated the reaction's enantioselectivity; however, the negligible difference between the two transition states was inconsistent with the experimental observations.

In the “SOA First” pathway (**Figure 5B**), the alkyl radical was added to the Ni^I species first, via a low energy barrier (**2-3_TS** 3.6 kcal/mol), forming the alkyl-Nphth-Ni^{II} intermediate **2-3**. Subsequently, the alkylboron radical was added to **2-3** on different faces, resulting in the formation of diastereomeric intermediates **3-1** and **3-2**. The following reductive elimination processes were identical to the third step in the “TM First” pathway. In the “SOA First” pathway, the enantio-determining step was also the alkylboron radical addition. The barrier for the *S*-configuration is 6.1 kcal/mol (**3-1_TS**), while it was 3.4 kcal/mol for the *R*-configuration (**3-2_TS**). The ΔΔG between the two transition states was 2.7 kcal/mol, indicating approximately 98% ee at room temperature, which was consistent with the experimental results. Compared to the “TM First” pathway, the “SOA First” pathway is more plausible.

To elucidate how the ligand controlled the enantioselectivity, we performed IGMH analysis[74,75] to visualize the weak interactions[76] in the two key transition states, **3-1_TS** and **3-2_TS**. The transition states were divided into three parts: the alkylboron radical, the alkyl nickel complex, and the phthalimide anion. The weak interaction isosurfaces are depicted in **Figure 5C**. The analysis clearly showed that the phthalimide anion bound to the nickel center through both an N-Ni coordinate bond and a hydrogen bond with the diamine ligand in both transition states. In **3-2_TS**, the pinacol moiety of the alkylboron radical formed a hydrogen bond with the chiral diamine ligand, with the methyl group of the alkylboron radical positioned in a manner to avoid steric hindrance from the bromine atom. Conversely, in **3-1_TS**, to mitigate the steric hindrance from the chiral ligand, the alkylboron radical adopted a different conformation, resulting in the loss of the hydrogen bond between the pinacol part and chiral diamine ligand. We hypothesized that the hydrogen bond predominantly governed the observed enantioselectivity.

To further rationalize the $Cp_2Zr^{III}Cl$ mediated reduction of NHPI esters, the DFT computations of this process was conducted. The results showed that the NHPI ester initially bound to the $Cp_2Zr^{III}Cl$ complex, forming a stable intermediate **RG_cpx** (**Figure 5D)**. The spin density plot revealed that the unpaired electron was primarily distributed to the phthalimide ring in **RG_cpx** intermediate. Subsequently, the homolytic cleavage of the N-O bond in **RG_cpx** occurred with a low energy barrier of 15.1 kcal/mol and a ΔG of -13.4 kcal/mol, indicating both thermodynamic and kinetic favorability. The computational analysis of the Zr-promoted NHPI ester reduction process supported our proposal and offered novel insights into

the generation of decarboxylation-derived radicals.

In conclusion, we have developed an asymmetric decarboxylative C(sp^3)-C(sp^3) cross-coupling reaction between primary aliphatic acids and *gem*-borazirconocene alkanes, providing a practical access to a broad range of valuable chiral alkylboron products using readily available primary aliphatic acids feedstocks. The high functional group tolerance allowed for late-stage modification of bioactive molecules and natural products with excellent enantioselectivity, highlighting the potential utility of this protocol. The intrinsic photoreactivity of alkylzirconocene reagents and their potential for enantioconvergent radical cross-coupling are harnessed in the asymmetric decarboxylative C(sp^3)-C(sp^3) cross-coupling reaction, offering a synthetically valuable strategy for photoredox chemistry.

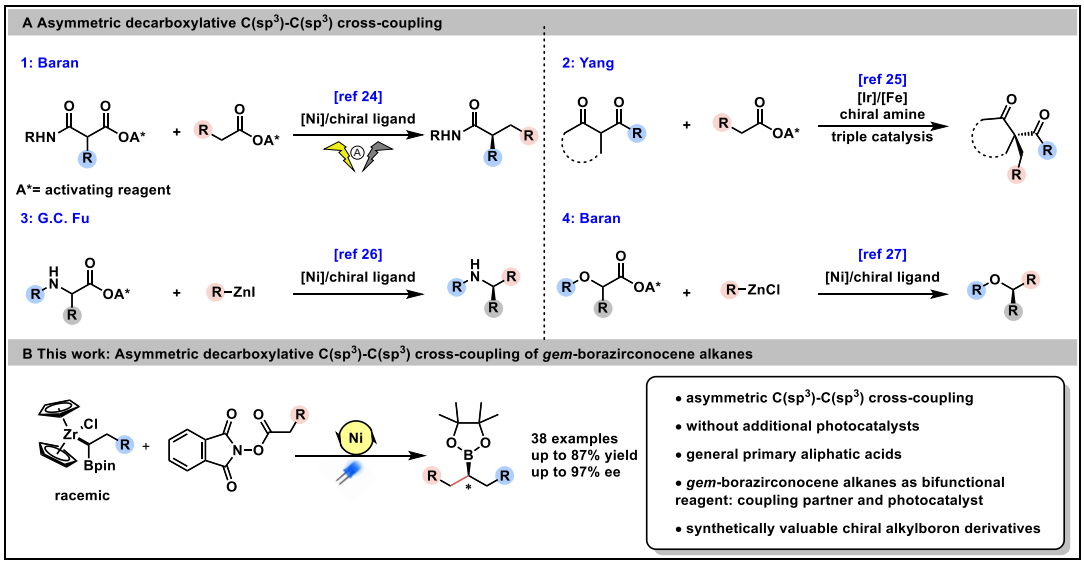

Figure 1: **Decarboxylative C(sp^3)-C(sp^3) cross coupling of alkyl carboxylic acids**. **A**: Previous asymmetric decarboxylative C(sp^3)-C(sp^3) cross-coupling. **B**: This work, Ni-catalyzed asymmetric decarboxylative C(sp^3)-C(sp^3) cross-coupling of *gem*-borazirconocene alkanes.

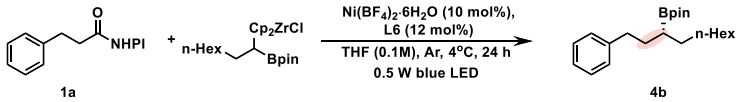

Entry	[a]condition	yield (%)	ee(%)
1	none	[b]82	91.6
2	w/o $Ni(BF_4)_2{\cdot}6H_2O$ and L6	N.D.	-
3	w/o light, and r.t.	N.D.	-
4	w/o Zr/B	N.D.	-
5	L1, instead of L6	80	53.0
6	L2, instead of L6	74	61.0
7	L3, instead of L6	84	79.5
8	L4, instead of L6	93	86.0
9	L5, instead of L6	53	67.0
10	L7, instead of L6	89	79.0

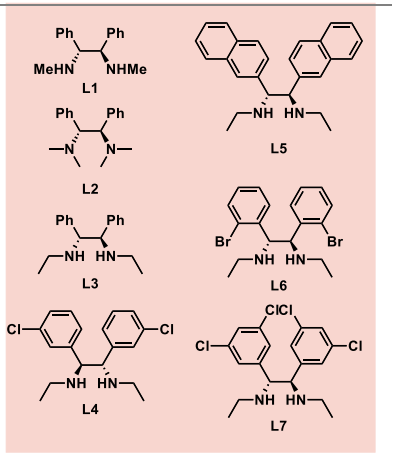

Table 1: Reaction development and optimization. All reactions were performed with $Ni(BF_4){\cdot}6H_2O$ (10 mol %), L6 (12 mol%), *gem*-borazirconocene alkanes (0.25 mmol), NHPI ester (0.1 mmol), and THF (1

mL), at 4°C with 0.5 W blue LEDs for 24 h. [a] Unless otherwise mentioned, all optimization reactions were carried out on a 0.1 mmol scale. The yields were determined by GC-MS analysis of the crude samples using dodecane as the internal standard. [b] The yield is the isolated yield (0.2 mmol scale). The ee value was detected by HPLC. N.D.: not detected.

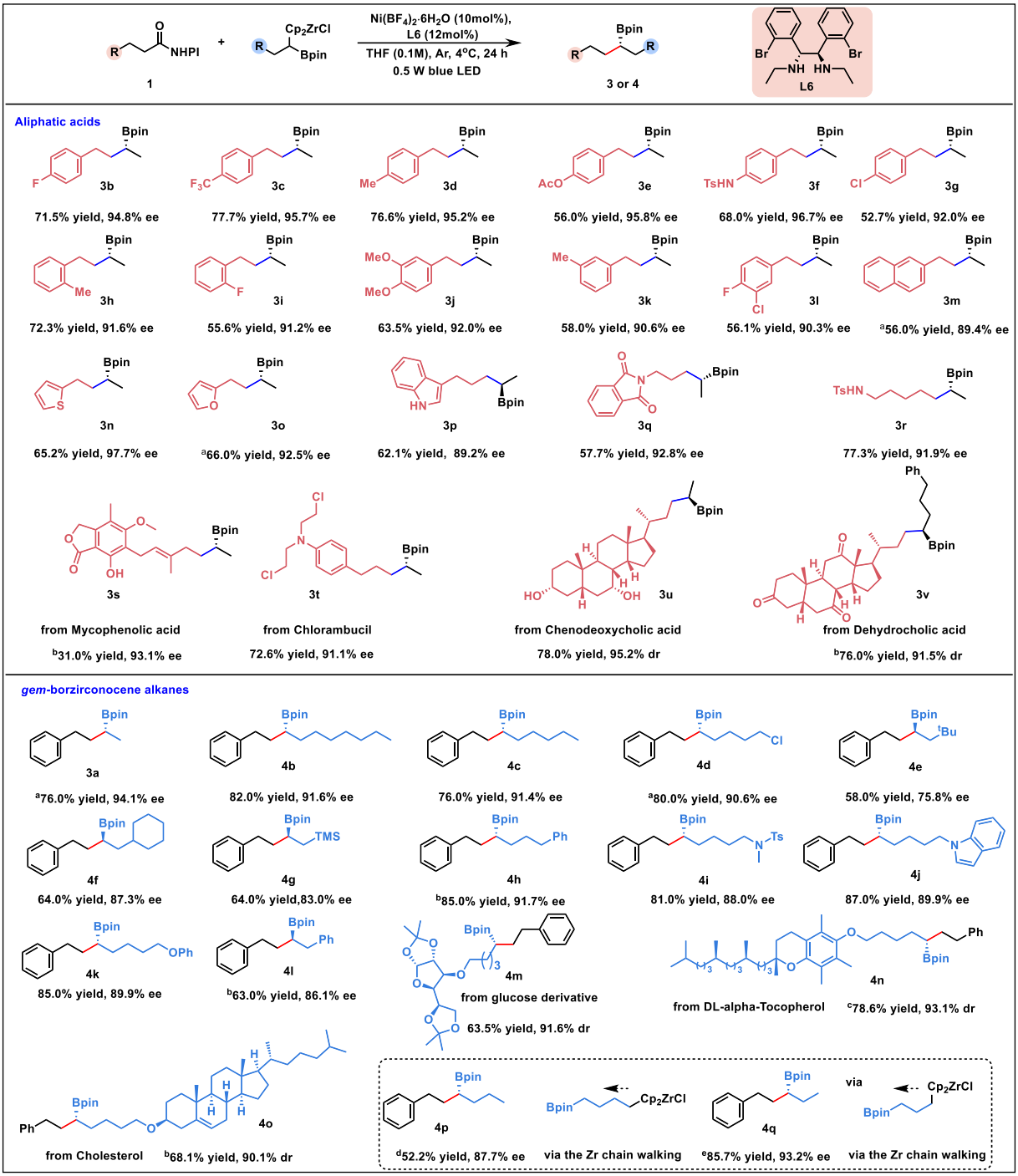

Figure 2: Scope of aliphatic acids and *gem*-borazirconocene alkanes. Unless otherwise mentioned, yields were isolated yields after purification by silica column chromatography, enantiomeric excess (ee) values were determined by HPLC analysis. All reactions were performed with $Ni(BF_4)\cdot 6H_2O$ (20 mol %), L6 (24 mol%), *gem*-borazirconocene alkanes (0.5 mmol), NHPI ester (0.2 mmol), and THF (2 mL), at 4°C with 0.5 W blue LEDs for 24 h. [a]: 3.7 equiv. *gem*-borazirconocene alkane was used. [b]: Isolated yields of the corresponding alcohol after oxidation. [c]: The isolated yields were total yields of two

diastereoisomers. [d]: 30% of starting material **2a** was recovered. [e]: 3.5 equiv. Cp_2ZrHCl was used.

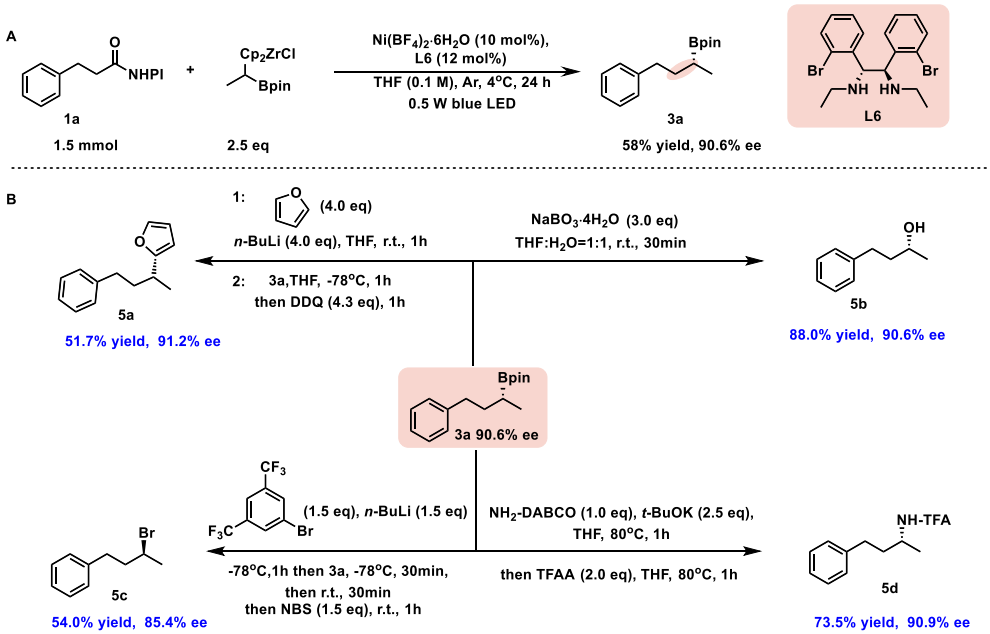

Figure 3: Gram-scale experiments and synthetic application. A: 1.5 mmol scale experiment. **B:** Synthetic applications of the chiral alkylboron products.

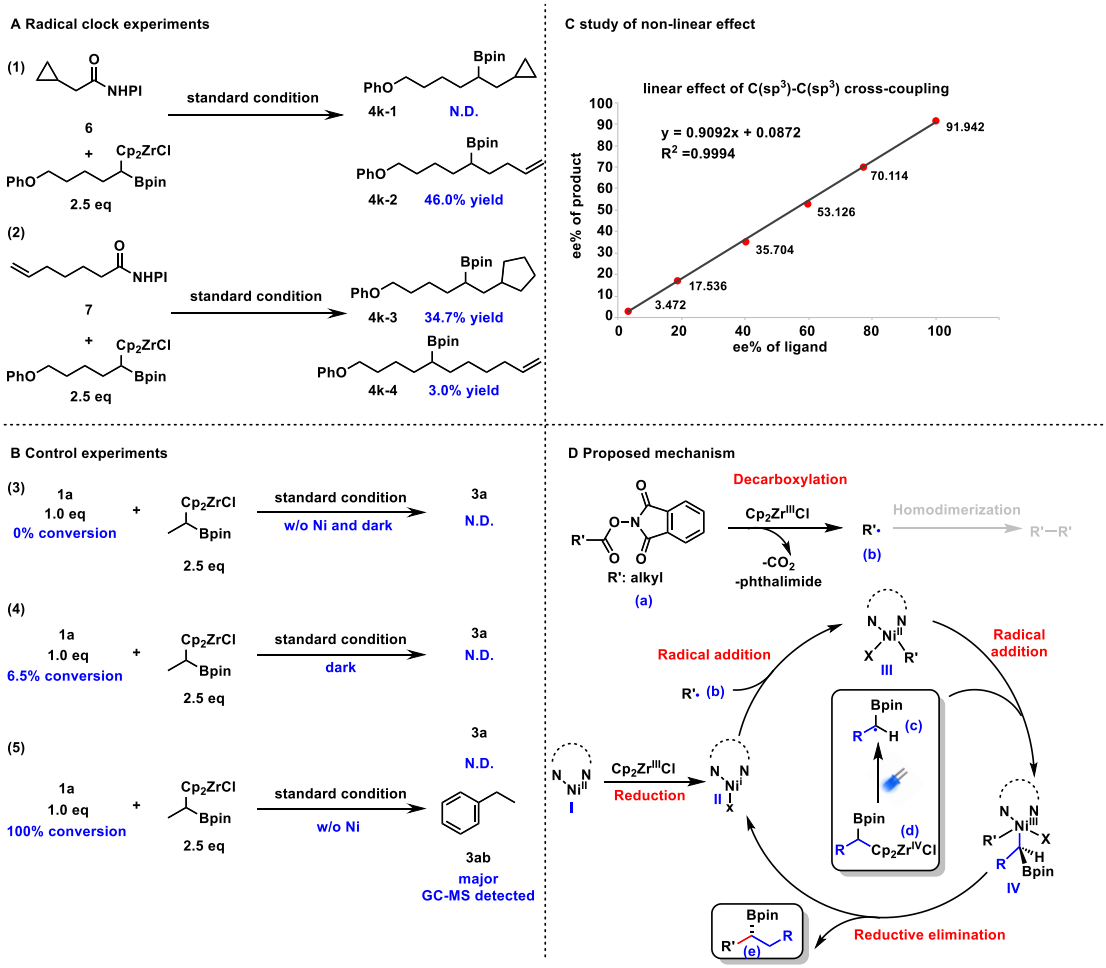

Figure 4: Mechanism studies. **A:** Radical clock experiment. **B:** Controlled experiments. **C:** Study of non-

linear effect. **D:** The proposed mechanism. N.D.: not detected.

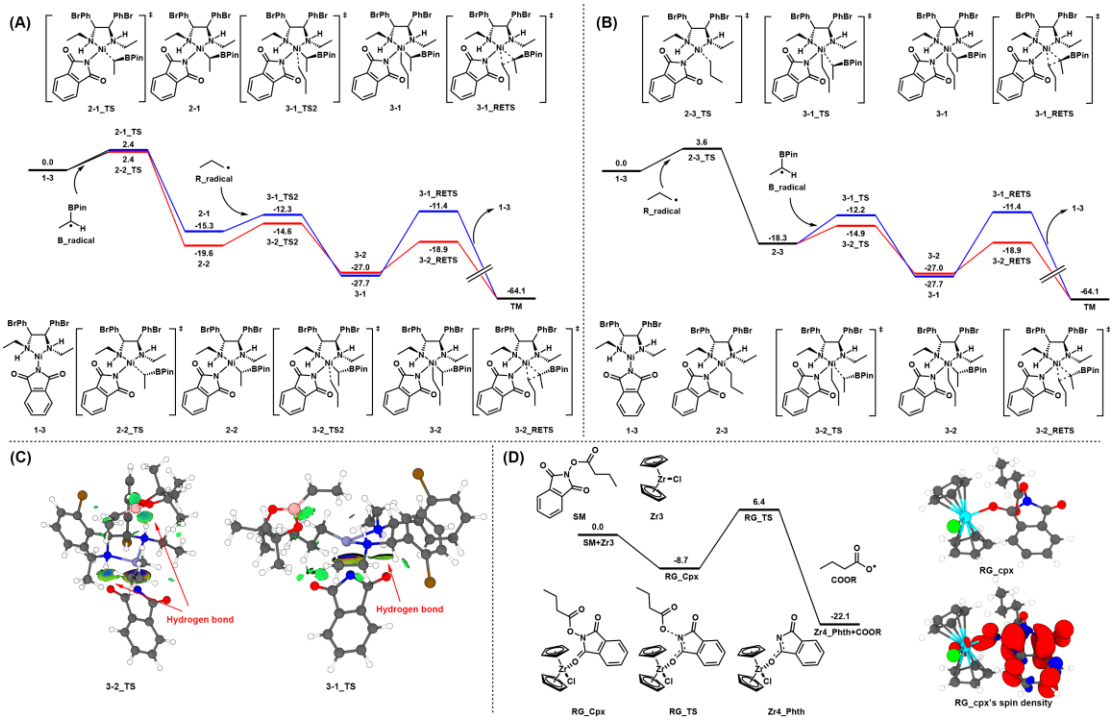

Figure 5. DFT study in reaction mechanism investigation. **A:** Reaction coordinate for "TM First" pathway, blue or red refer to absolute configuration of alkyl boron ester. (Blue for S, red for R) **B**: Reaction coordinate for "SOA First" pathway, blue or red refer to absolute configuration of alkyl boron ester. (Blue for S, red for R) **C**: Ball & stick model for **3-1_TS** and **3-2_TS** (color: red, O; gray, C; green, Cl; blue, N; white, H; ice blue, Ni; brown, Br; pink, B), with IGMH isosurface colored by sign (λ2) (colorbar: -0.05 a.u. to 0.05 a.u., blue to red) **D:** Reaction coordinate for Zr^{III}-mediated NHPI ester reduction (left), and spin density of ester-Zr^{III} complex (right, color: cyan, Zr; red, O; gray, C; green, Cl; blue, N; white, H).

Methods

General procedure for Ni-catalyzed asymmetric cross-coupling reaction

In an argon-filled glovebox, a flame-dried 4 mL sealing tube equipped with a Teflon septum and magnetic stir bar was charged with Cp_2ZrHCl (139.3 mg, 0.5 mmol, 2.7 equiv), the reaction vial was sealed tightly and removed from the glovebox, anhydrous THF (1.0 mL), alkenyl boronates (0.5 mmol, 2.5 equiv.) were added by a syringe under an argon atmosphere. The mixture was stirred at 50 °C for 1 h until a clear yellow solution was obtained. Another flame-dried 4 mL vial equipped with a Teflon septum and magnetic stir bar was charged with $Ni(BF_4)\cdot 6H_2O$ (6.8 mg, 0.02 mmol, 20 mol%), L6 (10.0 mg, 0.024 mmol, 24 mol%). The vial was sealed, and then evacuated and back-filled with argon (3 times). Then anhydrous THF (1.0 mL) was added under argon. Then the mixture was stirred for 1h at room temperature. Another flame-dried 4 mL sealing tube equipped with a Teflon septum and magnetic stir bar was charged with NHPI ester (0.2 mmol, 1.0 equiv.), the tube was sealed, and then evacuated and back-filled with argon (3 times). The previous clear alkyl zirconium boronates reagent and the nickel catalyst were successively transferred via syringe over 1 min to this reaction vial under an argon atmosphere. The reaction mixture was then stirred and irradiated with 0.5 W blue LEDs in the photoreactor at 4°C. After 24 h, the reaction mixture was concentrated in vacuum. Purification of the crude product by flash chromatography on silica gel afforded the desired product.

Data availability

The X-ray crystallographic coordinates for structures reported in this study have been deposited at the Cambridge Crystallographic Data Centre (CCDC), under deposition number 2347391 (**5b-1**) (https://dx.doi.org/10.5517/ccdc.csd.cc2jsn99). Copies of the data can be obtained free of charge via https://www.ccdc. cam.ac.uk/structures/. All other data supporting the findings of this study, including experimental procedures and compound characterization, NMR, and HPLC, computational information are available within the Article and its Supplementary Information or from the corresponding author upon request.

References

1. Tibbetts, J. D. *et al.* Decarboxylative, Radical C–C Bond Formation with Alkyl or Aryl Carboxylic Acids: Recent Advances. *Synthesis* **55**, 3239–3250 (2023).
2. Beil, S. B., Chen, T. Q., Intermaggio, N. E. & MacMillan, D. W. C. Carboxylic Acids as Adaptive Functional Groups in Metallaphotoredox Catalysis. *Acc. Chem. Res.* **55**, 3481–3494 (2022).
3. Laudadio, G., Palkowitz, M. D., El-Hayek Ewing, T. & Baran, P. S. Decarboxylative Cross-Coupling: A Radical Tool in Medicinal Chemistry. *ACS Med. Chem. Lett.* **13**, 1413–1420 (2022).
4. Zhu, X. & Fu, H. Photocatalytic cross-couplings via the cleavage of N–O bonds. *Chem. Commun.* **57**, 9656–9671 (2021).
5. Parida, S. K. *et al.* Single Electron Transfer-Induced Redox Processes Involving N-(Acyloxy)phthalimides. *ACS Catal.* **11**, 1640–1683 (2021).
6. Chen, H., Liu, Y. A. & Liao, X. Recent Progress in Radical Decarboxylative Functionalizations Enabled by Transition-Metal (Ni, Cu, Fe, Co or Cr) Catalysis. *Synthesis* **53**, 1–29 (2021).
7. Karmakar, S., Silamkoti, A., Meanwell, N. A., Mathur, A. & Gupta, A. K. Utilization of C(sp3)-Carboxylic Acids and Their Redox-Active Esters in Decarboxylative Carbon−Carbon Bond Formation. *Advanced Synthesis & Catalysis* **363**, 3693–3736 (2021).
8. McMurray, L., McGuire, T. M. & Howells, R. L. Recent Advances in Photocatalytic Decarboxylative Coupling Reactions in Medicinal Chemistry. *Synthesis* **52**, 1719–1737 (2020).
9. Konev, M. O. & Jarvo, E. R. Decarboxylative Alkyl–Alkyl Cross-Coupling Reactions. *Angewandte Chemie International Edition* **55**, 11340–11342 (2016).
10. Patra, T. & Maiti, D. Decarboxylation as the Key Step in C−C Bond-Forming Reactions. *Chemistry – A European Journal* **23**, 7382–7401 (2017).
11. Zhang, B. *et al.* Complex molecule synthesis by electrocatalytic decarboxylative cross-coupling. *Nature* (2023) doi:10.1038/s41586-023-06677-2.
12. Johnston, C. P., Smith, R. T., Allmendinger, S. & MacMillan, D. W. C. Metallaphotoredox-catalysed sp3–sp3 cross-coupling of carboxylic acids with alkyl halides. *Nature* **536**, 322–325 (2016).
13. Liu, W., Lavagnino, M. N., Gould, C. A., Alcázar, J. & MacMillan, D. W. C. A biomimetic SH2 cross-coupling mechanism for quaternary sp3-carbon formation. *Science* **374**, 1258–1263 (2021).
14. Tsymbal, A. V., Bizzini, L. D. & MacMillan, D. W. C. Nickel Catalysis via SH2 Homolytic Substitution: The Double Decarboxylative Cross-Coupling of Aliphatic Acids. *J. Am. Chem. Soc.* **144**, 21278–21286 (2022).
15. Sakai, H. A. & MacMillan, D. W. C. Nontraditional Fragment Couplings of Alcohols and Carboxylic Acids: C(sp3)–C(sp3) Cross-Coupling via Radical Sorting. *J. Am. Chem. Soc.* **144**, 6185–6192 (2022).
16. Zhang, B. *et al.* Ni-electrocatalytic Csp3–Csp3 doubly decarboxylative coupling. *Nature* **606**, 313–318 (2022).
17. Hioki, Y. *et al.* Overcoming the limitations of Kolbe coupling with waveform-controlled electrosynthesis.

Science **380**, 81–87 (2023).
18. Qin, T. *et al.* A general alkyl-alkyl cross-coupling enabled by redox-active esters and alkylzinc reagents. *Science* **352**, 801–805 (2016).
19. Gan, X. *et al.* Carbon quaternization of redox active esters and olefins by decarboxylative coupling. *Science* **384**, 113–118 (2024).
20. Lu, X., Xiao, B., Liu, L. & Fu, Y. Formation of C(sp3)–C(sp3) Bonds through Nickel-Catalyzed Decarboxylative Olefin Hydroalkylation Reactions. *Chemistry – A European Journal* **22**, 11161–11164 (2016).
21. Kang, K. & Weix, D. J. Nickel-Catalyzed C(sp3)–C(sp3) Cross-Electrophile Coupling of In Situ Generated NHP Esters with Unactivated Alkyl Bromides. *Org. Lett.* **24**, 2853–2857 (2022).
22. Zhang, Z. & Cernak, T. The Formal Cross-Coupling of Amines and Carboxylic Acids to Form sp3–sp3 Carbon–Carbon Bonds. *Angewandte Chemie International Edition* **60**, 27293–27298 (2021).
23. Bauer, T., Hakim, Y. Z. & Morawska, P. Recent Advances in the Enantioselective Radical Reactions. *Molecules* **28**, 6252 (2023).
24. Gao, Y., Zhang, B., He, J. & Baran, P. S. Ni-Electrocatalytic Enantioselective Doubly Decarboxylative C(sp3)–C(sp3) Cross Coupling. *J. Am. Chem. Soc.* (2023) doi:10.1021/jacs.3c03337.
25. Li, L.-J. *et al.* Enantioselective Construction of Quaternary Stereocenters via Cooperative Photoredox/Fe/Chiral Primary Amine Triple Catalysis. *J. Am. Chem. Soc.* (2024) doi:10.1021/jacs.4c01842.
26. Yang, Z.-P., Freas, D. J. & Fu, G. C. The Asymmetric Synthesis of Amines via Nickel-Catalyzed Enantioconvergent Substitution Reactions. *J. Am. Chem. Soc.* **143**, 2930–2937 (2021).
27. Gao, Y. *et al.* Ni-Catalyzed Enantioselective Dialkyl Carbinol Synthesis via Decarboxylative Cross-Coupling: Development, Scope, and Applications. *J. Am. Chem. Soc.* **144**, 10992–11002 (2022).
28. Knochel, Paul. & Singer, R. D. Preparation and reactions of polyfunctional organozinc reagents in organic synthesis. *Chem. Rev.* **93**, 2117–2188 (1993).
29. Jana, R., Pathak, T. P. & Sigman, M. S. Advances in Transition Metal (Pd,Ni,Fe)-Catalyzed Cross-Coupling Reactions Using Alkyl-organometallics as Reaction Partners. *Chem. Rev.* **111**, 1417–1492 (2011).
30. Xu, L. Decarboxylative Borylation: New Avenues for the Preparation of Organoboron Compounds. *European Journal of Organic Chemistry* **2018**, 3884–3890 (2018).
31. Grams, R. J. *et al.* The Rise of Boron-Containing Compounds: Advancements in Synthesis, Medicinal Chemistry, and Emerging Pharmacology. *Chem. Rev.* (2024) doi:10.1021/acs.chemrev.3c00663.
32. Marfavi, A., Kavianpour, P. & Rendina, L. M. Carboranes in drug discovery, chemical biology and molecular imaging. *Nat Rev Chem* **6**, 486–504 (2022).
33. Nguyen, V. D., Nguyen, V. T., Jin, S., Dang, H. T. & Larionov, O. V. Organoboron chemistry comes to light: Recent advances in photoinduced synthetic approaches to organoboron compounds. *Tetrahedron* **75**, 584–602 (2019).
34. Hu, J., Ferger, M., Shi, Z. & Marder, T. B. Recent advances in asymmetric borylation by transition metal catalysis. *Chem. Soc. Rev.* **50**, 13129–13188 (2021).
35. Ghosh, S., Ghosh, A., Pyne, P. & Hajra, A. Asymmetric C(sp3)–H borylation: an update. *Org. Biomol. Chem.* **20**, 4496–4511 (2022).
36. Li, Z. *et al.* Nickel-Catalyzed Regio- and Enantioselective Borylative Coupling of Terminal Alkenes with Alkyl Halides Enabled by an Anionic Bisoxazoline Ligand. *J. Am. Chem. Soc.* (2023) doi:10.1021/jacs.3c01040.

37. Zhou, J., Wang, D., Xu, W., Hu, Z. & XU, T. Enantioselective C(sp3)–C(sp3) Reductive Cross-Electrophile Coupling of Unactivated Alkyl Halides with α-Chloroboronates via Dual Nickel/Photoredox Catalysis. *J. Am. Chem. Soc.* **145**, 2081–2087 (2023).
38. Bera, S., Mao, R. & Hu, X. Enantioselective C(sp3)–C(sp3) cross-coupling of non-activated alkyl electrophiles via nickel hydride catalysis. *Nat. Chem.* **13**, 270–277 (2021).
39. Hu, D., Wang, L. & Li, P. Decarboxylative Borylation of Aliphatic Esters under Visible-Light Photoredox Conditions. *Org. Lett.* **19**, 2770–2773 (2017).
40. Li, C. *et al.* Decarboxylative borylation. *Science* **356**, eaam7355 (2017).
41. Fawcett, A. *et al.* Photoinduced decarboxylative borylation of carboxylic acids. *Science* **357**, 283–286 (2017).
42. Wang, J. *et al.* Cu-Catalyzed Decarboxylative Borylation. *ACS Catal.* **8**, 9537–9542 (2018).
43. Krokhmaliuk, Y., Kleban, I., Rassukana, Y. V. & Grygorenko, O. O. Organocatalytic Decarboxylative Borylation of Cyclopropane N-Hydroxyphthalimide Esters. *J. Org. Chem.* **89**, 2771–2776 (2024).
44. Serafino, A. *et al.* Visible-Light-Driven Decarboxylative Borylation: Rapid Access to α- and β-Amino-boronamides. *Org. Lett.* **25**, 9249–9254 (2023).
45. Wen, Q. *et al.* Iron-catalyzed decarbonylative borylation enables the one-pot diversification of (Hetero)Aryl and alkyl carboxylic acids. *Cell Reports Physical Science* **3**, 100995 (2022).
46. Dai, J.-J., Teng, X.-X., Fang, W., Xu, J. & Xu, H.-J. Electrochemically promoted decarboxylative borylation of alkyl *N*-hydroxyphthalimide esters. *Chinese Chemical Letters* **33**, 1555–1558 (2022).
47. Barton, L. M., Chen, L., Blackmond, D. G. & Baran, P. S. Electrochemical borylation of carboxylic acids. *Proceedings of the National Academy of Sciences* **118**, e2109408118 (2021).
48. Wei, D., Liu, T.-M., Zhou, B. & Han, B. Decarboxylative Borylation of mCPBA-Activated Aliphatic Acids. *Org. Lett.* **22**, 234–238 (2020).
49. Shu, X., Xu, R., Ma, Q. & Liao, S. Accessing alkyl boronic esters via visible light-mediated decarboxylative addition reactions of redox-active esters. *Organic Chemistry Frontiers* **7**, 2003–2007 (2020).
50. Zhang, Q. *et al.* Decarboxylative Borylation of Stabilized and Activated Carbon Radicals. *Angewandte Chemie International Edition* **59**, 21875–21879 (2020).
51. Mega, R. S., Duong, V. K., Noble, A. & Aggarwal, V. K. Decarboxylative Conjunctive Cross-coupling of Vinyl Boronic Esters using Metallaphotoredox Catalysis. *Angewandte Chemie International Edition* **59**, 4375–4379 (2020).
52. Noble, A., Mega, R. S., Pflästerer, D., Myers, E. L. & Aggarwal, V. K. Visible-Light-Mediated Decarboxylative Radical Additions to Vinyl Boronic Esters: Rapid Access to γ-Amino Boronic Esters. *Angewandte Chemie International Edition* **57**, 2155–2159 (2018).
53. Huang, M. *et al.* Photoredox/Cu-Catalyzed Decarboxylative C(sp3)–C(sp3) Coupling to Access C(sp3)-Rich gem-Diborylalkanes. *Angewandte Chemie International Edition* **n/a**, e202401782.
54. Maksymowicz, R. M., Roth, P. M. C. & Fletcher, S. P. Catalytic asymmetric carbon–carbon bond formation using alkenes as alkylmetal equivalents. *Nature Chem* **4**, 649–654 (2012).
55. You, H., Rideau, E., Sidera, M. & Fletcher, S. P. Non-stabilized nucleophiles in Cu-catalysed dynamic kinetic asymmetric allylic alkylation. *Nature* **517**, 351–355 (2015).
56. Maksymowicz, R. M., Bissette, A. J. & Fletcher, S. P. Asymmetric Conjugate Additions and Allylic Alkylations Using Nucleophiles Generated by Hydro- or Carbometallation. *Chemistry – A European Journal* **21**, 5668–5678 (2015).
57. Wipf, P. & Xu, W. Organozirconocenes in organic synthesis: tandem epoxide rearrangement-carbonyl

addition. *J. Org. Chem.* **58**, 825–826 (1993).
58. Wipf, P. & Pierce, J. G. Synthesis of Homoallylic Amines by Hydrozirconation−Imine Addition of Allenes. *Org. Lett.* **7**, 3537–3540 (2005).
59. Masarwa, A. *et al.* Merging allylic carbon–hydrogen and selective carbon–carbon bond activation. *Nature* **505**, 199–203 (2014).
60. Yang, C., Jiang, C. & Qi, X. Alkylzirconocenes in Organic Synthesis: An Overview. *Synthesis* **53**, 1061–1076 (2021).
61. Némethová, I. & Šebesta, R. Are Organozirconium Reagents Applicable in Current Organic Synthesis? *Synthesis* **53**, 447–460 (2021).
62. Pinheiro, D. L. J., de Castro, P. P. & Amarante, G. W. Recent Developments and Synthetic Applications of Nucleophilic Zirconocene Complexes from Schwartz's Reagent. *European Journal of Organic Chemistry* **2018**, 4828–4844 (2018).
63. Gao, Y. *et al.* Visible-Light-Induced Nickel-Catalyzed Cross-Coupling with Alkylzirconocenes from Unactivated Alkenes. *Chem* **6**, 675–688 (2020).
64. Yang, C., Bai, S., Gao, Y., Wu, Q. & Qi, X. Visible-light-induced enantioselective radical cross-coupling of C(sp3)-borazirconocene. *Chem* (2023) doi:10.1016/j.chempr.2023.04.006.
65. Hirao, Y., Katayama, Y., Mitsunuma, H. & Kanai, M. Chromium-Catalyzed Linear-Selective Alkylation of Aldehydes with Alkenes. *Org. Lett.* **22**, 8584–8588 (2020).
66. Ren, X., Gao, X., Min, Q.-Q., Zhang, S. & Zhang, X. (Fluoro)alkylation of alkenes promoted by photolysis of alkylzirconocenes. *Chem. Sci.* **13**, 3454–3460 (2022).
67. Yang, C., Gao, Y., Bai, S., Jiang, C. & Qi, X. Chemoselective Cross-Coupling of gem-Borazirconocene Alkanes with Aryl Halides. *J. Am. Chem. Soc.* **142**, 11506–11513 (2020).
68. Sandford, C. & Aggarwal, V. K. Stereospecific functionalizations and transformations of secondary and tertiary boronic esters. *Chem. Commun.* **53**, 5481–5494 (2017).
69. Odachowski, M. *et al.* Development of Enantiospecific Coupling of Secondary and Tertiary Boronic Esters with Aromatic Compounds. *J. Am. Chem. Soc.* **138**, 9521–9532 (2016).
70. Liu, X. *et al.* Aminoazanium of DABCO: An Amination Reagent for Alkyl and Aryl Pinacol Boronates. *Angewandte Chemie International Edition* **59**, 2745–2749 (2020).
71. Larouche-Gauthier, R., Elford, T. G. & Aggarwal, V. K. Ate Complexes of Secondary Boronic Esters as Chiral Organometallic-Type Nucleophiles for Asymmetric Synthesis. *J. Am. Chem. Soc.* **133**, 16794–16797 (2011).
72. Cornella, J. *et al.* Practical Ni-Catalyzed Aryl–Alkyl Cross-Coupling of Secondary Redox-Active Esters. *J. Am. Chem. Soc.* **138**, 2174–2177 (2016).
73. Turro, R. F. *et al.* Mechanistic Investigation of Ni-Catalyzed Reductive Cross-Coupling of Alkenyl and Benzyl Electrophiles. *J. Am. Chem. Soc.* (2023) doi:10.1021/jacs.3c02649.
74. Lu, T. & Chen, Q. Independent gradient model based on Hirshfeld partition: A new method for visual study of interactions in chemical systems. *J Comput Chem* **43**, 539–555 (2022).
75. Lu, T. & Chen, Q. Erratum to "Independent gradient model based on Hirshfeld partition: A new method for visual study of interactions in chemical systems". Preprint at https://doi.org/10.26434/chemrxiv-2022-g1m34 (2022).
76. Lu, T. & Chen, F. Multiwfn: A multifunctional wavefunction analyzer. *J Comput Chem* **33**, 580–592 (2012).

Acknowledgements

This work was supported by the National Natural Science Foundation of China (grant no. 82225041, X.Q.).

We thank Dr. Zhen Liu for his scientific suggestions for this manuscript. The authors gratefully acknowledge the Beijing Municipal Government and Tsinghua University for their financial support.

Author contributions

X.Q. conceived of the study; J.W. carried out most of the reactions and prepared supplemental information; J.W., S.B. and X.Q. prepared the manuscript; S.B. performed DFT computation; J.W. and X.Q. analyzed the data; All authors discussed the results and commented on the manuscript.

Competing interests

The authors declare no competing interests.

Graphical abstract